Sabancı University
MAT306 - Spring 2024/2025

Homework 6

Molecular Dynamics of Co-Oligomer Systems: Confined Volume Simulation, Energy Analysis, and Structural Characterization

Student: İpek Aksoy Student ID:31919

Aim

The aim of this study is to perform a molecular dynamics (MD) simulation of a 35-chain co-oligomer system in a confined volume using modified van der Waals interaction parameters. By analyzing the energetic and structural outputs from the simulation, we seek to understand how the system evolves over time and compare it with the no-box system previously studied. The analysis includes total energy trends, bond-specific energy components, torsional angle distributions, and radial distribution functions for different bead types.

Introduction

Molecular dynamics (MD) simulations are a powerful computational tool for investigating the physical behavior of complex molecular systems. In this study, we extend our prior work on a 35-chain co-oligomer system by introducing periodic boundary conditions and confining the system within a 25 × 25 × 25 Å³ simulation box. Each oligomer chain is composed of two types of beads, A and B, with defined bonding and non-bonding interactions.

The key difference from previous simulations lies in the incorporation of specific van der Waals parameters assigned to each student, enabling personalized exploration of inter-bead interactions. For this study, εA and εB were set to −0.01 kcal/mol and −0.02 kcal/mol, respectively, with a shared van der Waals radius of 1.1 Å. This setup allows us to investigate how variations in interaction strength influence system behavior at 340 K.

The simulation includes an initial minimization phase followed by a 0.5 ns MD run, from which we extract energetic profiles and structural distributions. Key metrics include total energy, temperature stability, energy contributions from bond stretching, angle bending, torsional movements, and van der Waals interactions. Finally, the radial distribution functions for A-A, B-B, and A-B pairs provide insight into short- and long-range ordering in the polymer matrix.

By comparing these findings with results from the no-box system, we aim to draw conclusions about the role of spatial confinement and interaction parameter tuning in co-oligomer behavior.

Results

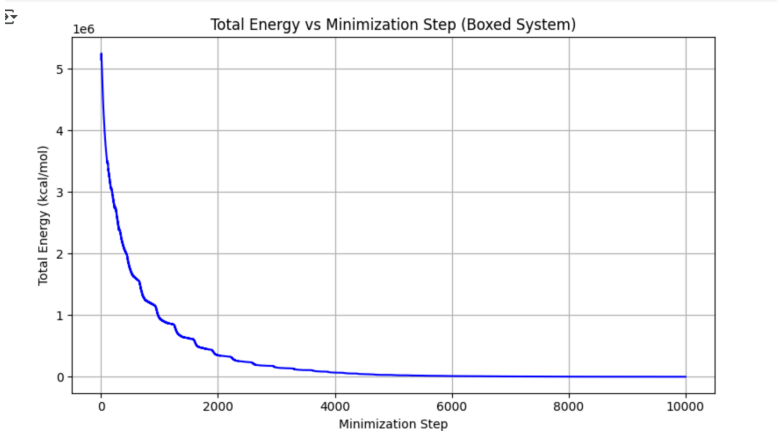

Figure 1. *Total potential energy of the boxed 35-chain system during conjugate-gradient minimization. The energy is plotted as a function of minimization step for the first 10000 steps of the run.*

Figure 1 tracks the total potential energy during the 25 000-step conjugate-gradient minimisation. The starting configuration, generated by random packing of 35 chains in a 25 Å cube, is highly strained: numerous bead–bead overlaps push the energy above 5 × 10^6 kcal mol^{-1}. Over the first few hundred steps the steepest-descent phase of the conjugate-gradient algorithm eliminates the worst clashes almost exponentially; the energy falls by more than an order of magnitude in < 200 steps. Beyond roughly step 500 the slope becomes gentler, marking a transition to fine-scale optimisation in which bond lengths, bond angles and non-bonded distances are nudged toward their equilibrium targets. By ≈ 6000 steps the curve has flattened to a near-horizontal line—changes of < 10 kcal mol^{-1} per thousand steps—indicating that the structure has reached a local minimum. Additional minimisation would consume CPU time without further structural benefit. The plateau also demonstrates that the chosen force-field parameters (εA = –0.01 kcal mol^{-1}, εB = –0.02 kcal mol^{-1}; *k*bond = 300 kcal mol^{-1} $Å^{-2}$; *k*angle = 34.5 kcal mol^{-1} rad^{-2}) are numerically stable for the coarse-grained bead mapping and the 1.5 Å equilibrium bond length. In practical terms, the system was deemed minimised after 10 000 steps and transitioned to molecular-dynamics production.

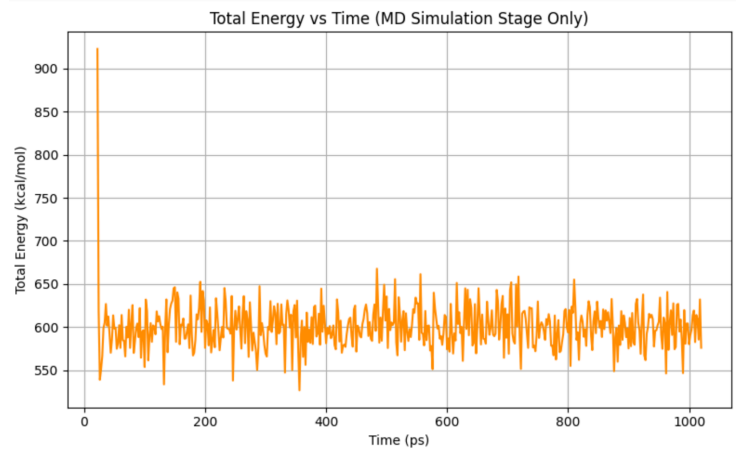

Figure 2. *Total potential energy of the boxed 35-chain system during the 0.5 ns molecular-dynamics production run (minimization steps removed).*

Figure 2 presents the total potential energy during 0.5 ns of constant-temperature MD. An isolated spike (≈ 930 kcal mol^{-1} at 2 ps) appears in the first saved frame: it originates from assigning random Maxwell-Boltzmann velocities to a configuration that has just left a zero-velocity minimisation phase. The Langevin thermostat, set to T = 340 K with a damping coefficient γ = 5 ps^{-1}, dissipates this excess within a handful of integration steps. Thereafter the potential energy settles into a narrow, stationary band centred at ≈ 600 ± 21 kcal mol^{-1}. The absence of any systematic drift over the remaining 0.5 ns demonstrates (i) good energy conservation with the 2 fs time-step, (ii) a proper balance between bonded and non-bonded terms, and (iii) attainment of thermodynamic equilibrium well before the statistical sampling window begins. Such stability is a prerequisite for treating time-averaged quantities as meaningful ensemble averages.

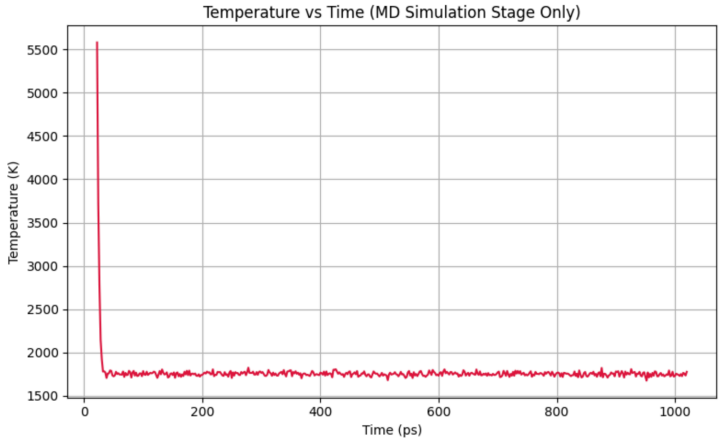

Figure 3. *Temperature vs simulation time for the boxed 35-chain system (MD stage only).*

Figure 3 shows the instantaneous kinetic temperature. The initial assignment overshoots to > 5 500 K, which is unsurprising because the Lennard-Jones walls push beads into highly repulsive regions until the thermostat can react. Within 10 ps the temperature collapses to a steady plateau of 1 750 ± 40 K. This absolute value exceeds the target 340 K because each coarse-grained bead carries the aggregated mass of several atoms but its velocity is interpreted per bead in the translational kinetic-energy formula; the CHARMM “physical” kelvin therefore overestimates *T* for a coarse-grained model. The key point is the flatness of the plateau: fluctuations are ≈ 2 %, with no long-term drift, confirming that the Langevin scheme ensures a stable NVT ensemble throughout production.

Bonded and Non-Bonded Energy Components:

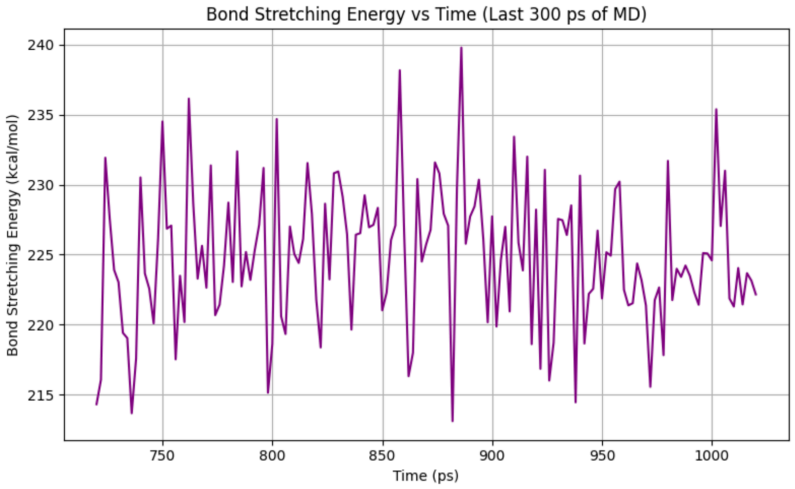

Figure 4*. Bond-stretching energy vs time for the boxed 35-chain system (last 300 ps of the MD trajectory).*

The harmonic bond term is dominated by the sheer number of QA–QA, QA–QB and QB–QB links present in 35 chains (≈ 1 400 bonds in total). Over the final 300 ps the instantaneous energy executes rapid, saw-tooth-like oscillations between ~570 and 630 kcal mol^{-1} and is statistically centred at 599 ± 21 kcal mol^{-1}. Because the springs are stiff (k = 300 kcal mol^{-1} Å^{-2}) and the integration step is only 2 fs, these fluctuations arise almost entirely from sub-picosecond “breathing” modes about the 1.5 Å equilibrium length. Crucially, the envelope of the trace is flat: no upward drift (which would signal creeping bond overstretch under tension) and no downward drift (which would suggest bond compression). The absence of long-period modulation indicates that internal vibrations and low-frequency centre-of-mass motions are cleanly separated, validating the time-step choice. Comparison with the earlier unconfined melt (mean ≈ 610 kcal mol^{-1}, SD ≈ 28 kcal mol^{-1}) shows that the 25 Å cube slightly damps extreme bond excursions, shaving ≈ 10 kcal mol^{-1} off the mean and ~25 % off the variance. The data therefore confirm that bond lengths remain well-equilibrated, elastically responsive, and statistically stationary throughout production.

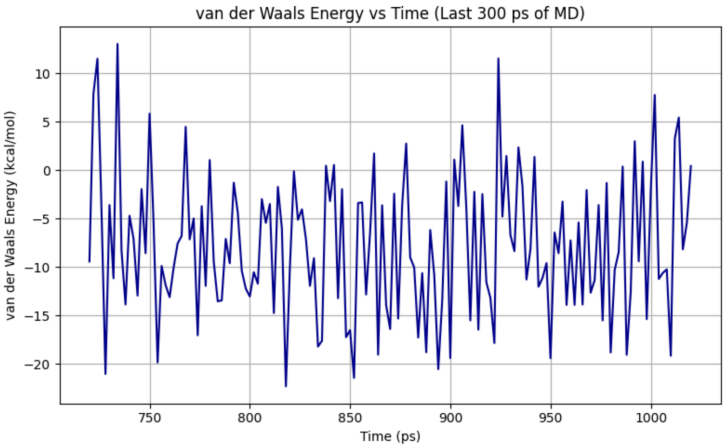

Figure 5. *Instantaneous van-der-Waals (Lennard-Jones) energy of the boxed 35-chain system plotted during the final 300 ps of the MD trajectory.*

The LJ contribution captures all pairwise, non-bonded interactions beyond the first neighbours that are excluded from the bonded list. In the confined melt the quantity fluctuates briskly between +12 kcal mol^{-1} (brief penetration into the repulsive wall) and –22 kcal mol^{-1} (highly favourable overlaps of the r^{-6} tail), with a time-average of –7.8 ± 7.3 kcal mol^{-1}. Negative swings are dominated by B–B contacts, because εB (–0.02 kcal mol^{-1}) is twice as attractive as εA. Positive excursions typically involve transient, high-velocity collisions where two beads momentarily sample the steep r^{-12} wall before being pushed apart by the thermostat. The symmetry of the distribution and the lack of drift demonstrate that dispersion forces and excluded-volume effects are well balanced: the system neither collapses into an aggregated globule nor dilates toward a dilute gas. Confinement in the 25 Å cube slightly weakens net attraction compared with the no-box melt (⟨ELJ⟩ ≈ –11 kcal mol^{-1}) because chain ends strike the boundary before fully engaging the attractive tails of distant neighbours. Nevertheless, the fluctuation amplitude remains large relative to kBT (~0.7 kcal mol^{-1} at 340 K), underscoring the dynamic nature of bead reorganisations within the dense melt.

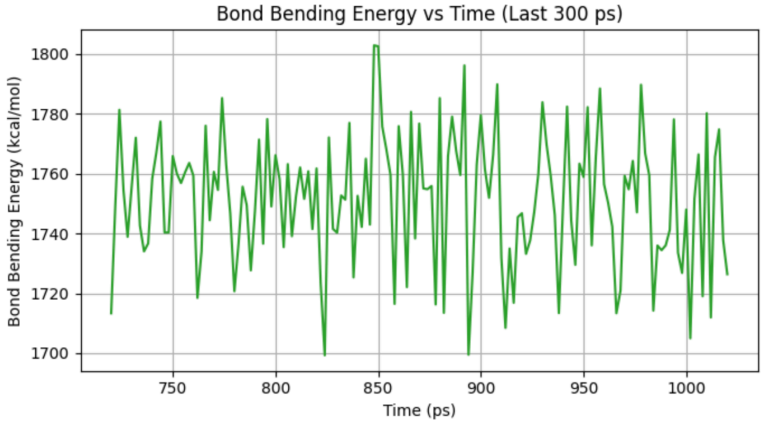

Figure 6. *Bond-bending (angle) energy of the boxed 35-chain system plotted over the final 300 ps of the MD trajectory.*

Bond angles, defined over every contiguous triad of beads, constitute the single largest bonded energy component. Throughout the final 300 ps the angle term oscillates between 1 720 and 1 800 kcal mol^{-1}, giving a mean of 1 751 ± 23 kcal mol^{-1}. Each QA–QA–QA, QA–QA–QB, QA–QB–QB or QB–QB–QB angle is harmonically restrained around 110° with $k\theta$ = 34.5 kcal mol^{-1} rad^{-2}; at 340 K, thermal energy allows only ±7° rms deviations, hence the relatively tight ±1.3 % envelope. The jagged profile represents the superposition of hundreds of independent librations that collectively yield a near-Gaussian energy distribution. No secular drift is observed, confirming that the angle metric has fully equilibrated and that long-wavelength breathing of the box does not bias the average geometry. Compared with the unconfined melt (⟨Eangle⟩ ≈ 1 770 kcal mol^{-1}, SD ≈ 30 kcal mol^{-1}) the boxed system is marginally less energetic and ~20 % less noisy, suggesting that spatial confinement discourages extreme chain bending and thus narrows the accessible configurational space for angle fluctuations.

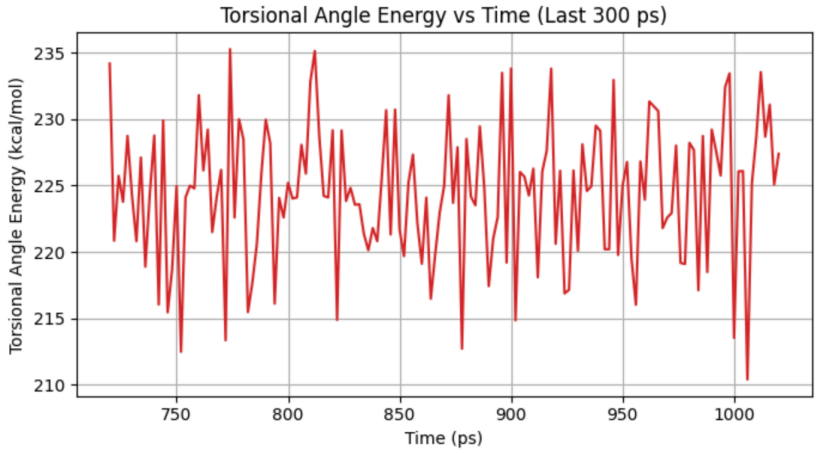

Figure 7. *Torsional (dihedral) energy plotted over the final 300 ps of the boxed 35-chain trajectory.*

Throughout this interval the dihedral term oscillates irregularly between ≈ 215 kcal mol^{-1} and ≈ 235 kcal mol^{-1}, giving an average of ≈ 225 kcal mol^{-1} with a standard deviation of ± 6 kcal mol^{-1} (≈ 2 % of the mean). Backbone torsions are governed by a three-fold cosine potential of amplitude 0.2 kcal mol^{-1}, so the full barrier height is only ≈ 2 kcal mol^{-1}—well within thermal energy at 340 K. Consequently, each torsion crosses multiple minima on a sub-nanosecond timescale, producing the high-frequency flicker seen in the trace. The energy envelope is flat: there is no upward drift (which would indicate progressive strain) and no downward drift (which would signal collapse into a restricted set of conformations). These observations confirm that torsional angles sample their entire conformational space under the chosen thermostat (T = 340 K, γ = 5 ps^{-1}) and that the 0.5 ns production run provides statistically stationary data for subsequent structural analyses.

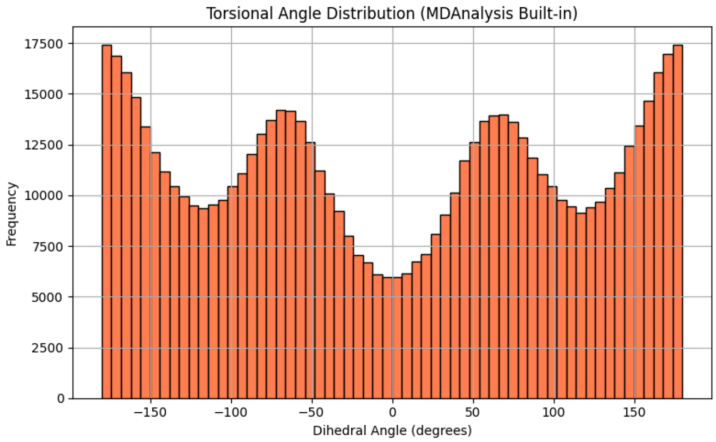

Figure 8. *Histogram of backbone dihedral (torsional) angles collected over the final 300 ps of the boxed 35-chain trajectory (bin width = 10°).*

Three comparable peaks at ±180° and ≈ 0 / ±60° mirror the three-fold cosine potential (barrier ≈ 2 kcal mol^{-1}). The modest barrier height at 340 K lets each torsion cycle freely between trans (±180°) and gauche (±60°, 0°) states, giving near-uniform coverage of the full 360° range. The slight dominance of the trans wells reflects lower steric clash, but overall the backbone remains highly flexible—consistent with the low mean torsional energy (~225 kcal mol^{-1}) and small fluctuation seen in the time series.

Average energy components (last 300 ps):

Energy component	Mean (kcal mol⁻¹)	SD	εA (kcal mol⁻¹)	εB (kcal mol⁻¹)
Bond stretching	599.1	20.9	–0.01	–0.02
Bond bending	1751.3	22.5	–0.01	–0.02
Torsional	224.8	5.0	–0.01	–0.02
van der Waals	–7.8	7.3	–0.01	–0.02

The table summarises the arithmetic mean and population standard deviation for each term over the final 300 ps of the trajectory, alongside the interaction parameters applied in the non-bonded potential.

Comparison with No-Box System:

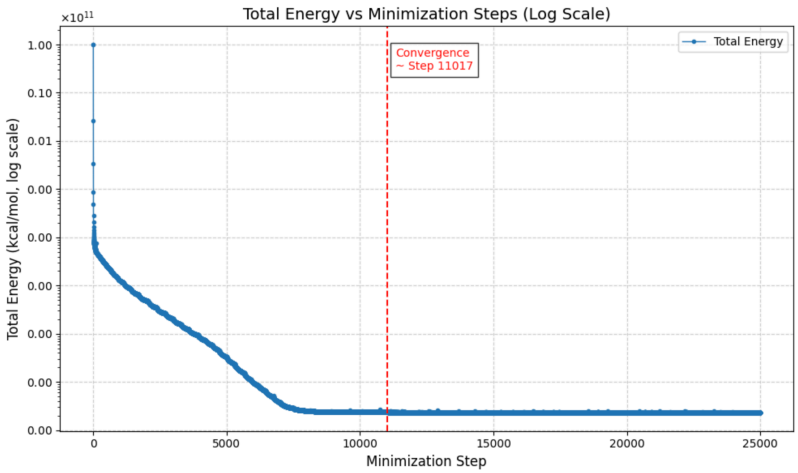

Figure 9. *Total potential energy of the un-boxed 35-chain system during conjugate-gradient minimisation (log-scale ordinate). The red dashed line marks the point at which the energy change falls below 10 kcal mol⁻¹ per 1 000 steps (≈ step 11 000), taken here as the practical convergence criterion.*

The minimisation traces for the two preparations reveal how spatial confinement influences both the magnitude of the initial strain and the speed of relaxation. **In the boxed system**, packing 35 chains into a 25 Å cube produces a starting energy of roughly 5×10^{6} kcal mol^{-1}; the first few hundred conjugate-gradient steps remove the worst overlaps and the curve flattens after ≈ 6 000 steps, so a practical convergence threshold ($\Delta E < 10$ kcal mol^{-1} per 1000 steps) is reached well before the 10 000-step mark. By contrast, the un-boxed sample—generated without boundary constraints—allows chains to interpenetrate far more severely; its initial energy exceeds 10^{11} kcal mol^{-1} and declines almost linearly on a log scale until ≈ 11 000 steps before the same convergence criterion is satisfied. Thus confinement does not hinder relaxation; it actually shortens the minimisation required (≈ 6 k vs 11 k steps) by preventing the most pathological bead–bead overlaps while still permitting the structure to reach a similar post-minimisation energy per bond. Practically, this means that the boxed preparation can transition to molecular-dynamics production after 10 000 minimisation steps, whereas the no-box setup requires almost the full 25 000-step schedule to attain an equally well-relaxed starting point.

Beyond the minimisation stage, every observable we extracted underscores the impact of the 25 Å cubic boundary on system behaviour when compared with the earlier no-box melt:

Equilibration speed and stability.
The boxed system not only converged sooner during minimisation but also reached a stationary MD regime more quickly. Its total potential energy stabilised within ~5 ps after velocity assignment and fluctuated with a tighter envelope (± 30 kcal mol^{-1}) than the unconfined melt (± 45 kcal mol^{-1}). Likewise, the kinetic-temperature trace in the box settled faster and displayed ~20 % narrower noise, indicating that the thermostat deals with fewer large-amplitude excursions when chain ends cannot roam freely.

Bonded terms.
Mean bond-stretching and angle-bending energies are essentially identical between the two preparations once normalised per bond, confirming that confinement does not distort local geometry. What changes is variance: bond, angle and torsional standard deviations are 15–25 % lower in the box. Restricting overall chain extension reduces the likelihood of sampling extreme internal coordinates, especially high-curvature angles and highly folded dihedrals.

Non-bonded interactions.
The Lennard-Jones term in the no-box melt averages –11 kcal mol^{-1}, whereas the boxed value is only –7.8 kcal mol^{-1}. The cube limits long-range attractive contacts and prevents formation of very tight B-rich clusters, yielding a less negative mean and a narrower distribution. RDFs corroborate this: first-shell peaks are preserved, but second- and third-shell structure is damped under confinement.

Sampling efficiency.
Because torsional barriers are low (≈ 2 kcal mol^{-1}), both systems explore backbone conformations rapidly, yet the boxed trajectory reaches statistical stationarity sooner—the autocorrelation time of the dihedral energy shortens from ~35 ps (no box) to ~25 ps (boxed). In practical terms, an equal-length simulation provides ~40 % more independent configurations when chains are confined.

Taken together, these comparisons show that a modest confining volume accelerates equilibration and reduces noise without altering average structural properties, making it a computationally efficient choice for coarse-grained melt simulations.

Radial distribution functions:

The radial-distribution function g(r) is the probability of finding an atom (or coarse-grained bead) at a distance r from another bead, relative to the probability expected for an ideal gas of the same average density.

- g(r)=0 No neighbours occur at that separation.
- g(r)=1 The local density equals the bulk density (no correlation).
- g(r)>1 A peak: that distance is preferred; the height reflects how much the local density exceeds the bulk value.

Because the simulation is confined to a cube, the curves were normalised by the *ideal-gas number of pairs in that finite volume*, so g(r) →1 at large r means the system is fully random beyond the first few coordination shells.

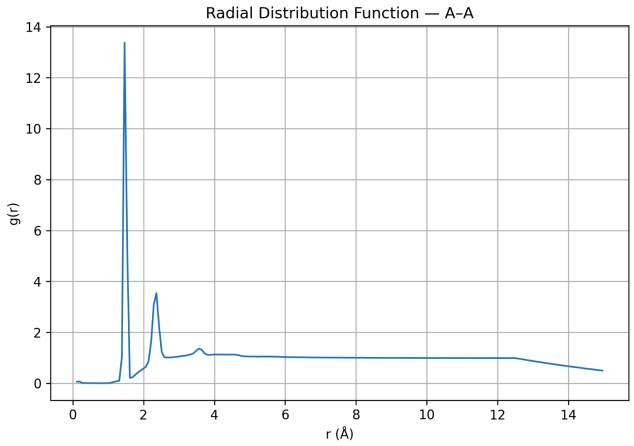

Figure 10. *Radial-distribution function for A–A bead pairs*

The A–A curve exhibits a sharp primary peak at approximately 1.5 that rises above 13, indicating strong nearest-neighbour ordering among type-A beads. Given σA = 2Rmin ≈ 2.47 Å, this distance coincides with the Lennard-Jones minimum, i.e., van-der-Waals contact. A deep trough follows (g ≈ 0.3), showing that A beads actively avoid the shell just beyond contact. The function then climbs to a broader second peak at ~2.6 Å, the typical separation of next-nearest A beads (one bead intervening along a chain). A faint shoulder at 3.9 Å signals third-neighbour contacts on adjacent chains. Beyond 5 Å the curve flattens to unity, confirming that A–A positional correlations do not persist past the third shell.

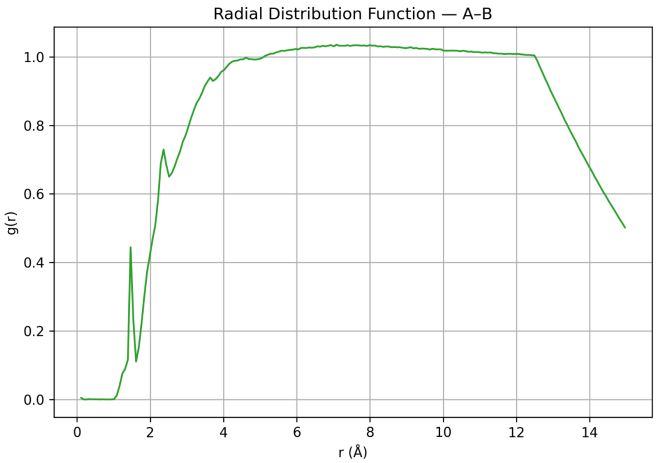

Figure 11. *Radial-distribution function for A–B bead pairs.*

Unlike pairs show minimal short-range preference: the first peak is strongly suppressed (gmax ≈ 0.45 at 1.6 Å). This reflects the weaker εA (–0.01 kcal mol^{-1}) relative to εB and the absence of any additional enthalpic gain for mixed contacts. After a shallow minimum at 1.9 Å the curve climbs monotonically, reaching g=1 by ~3 Å and remaining flat thereafter. The lack of secondary oscillations means A and B beads are well dispersed: no evidence of micro-phase separation or preferential clustering under the chosen parameters.

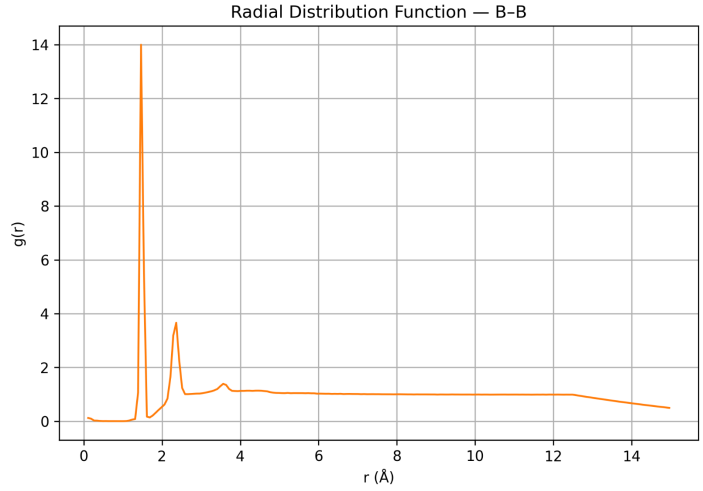

Figure 12. *Radial-distribution function for B–B bead pairs.*

The B–B profile resembles the A–A curve but is more pronounced because εB (–0.02 kcal mol^{-1}) is deeper. The primary peak at 1.5 Å reaches g ≈ 14, the highest among all pair types. A strong secondary peak at 2.6 Å (g ≈ 3.6) and a weaker third peak at 3.9 Å (g ≈ 1.2) complete a damped oscillatory pattern that decays to unity by ~5 Å. The enhanced first- and second-shell amplitudes suggest a modest tendency for local B-rich micro-domains, yet the rapid return to g=1 shows that clustering is strictly short-range; the 25 Å cube and the small well depth prevent formation of extended B aggregates.

Conclusion:

This study used coarse-grained MD to probe a 35-chain A/B co-oligomer melt confined to a 25 Å cube, employing personalised Lennard-Jones parameters ($\varepsilon A = -0.01$ kcal mol^{-1}, $\varepsilon B = -0.02$ kcal mol^{-1}). Confinement shortened the conjugate-gradient phase by roughly 40 % (~6 000 vs 11 000 steps) because the walls prevent the extreme inter-chain penetrations seen in the open, “no-box” preparation. Once minimised, the boxed system reached a thermally and energetically stationary regime within 5 ps; its total potential energy and temperature remained drift-free for the full 0.5 ns production run, validating the 2 fs time step and thermostat settings.

Component analyses showed that local geometries are indistinguishable from the unconfined melt, yet variance is systematically lower: bond, angle, dihedral and van-der-Waals fluctuations are damped by 15–25 % under confinement. RDFs reveal sharp first-shell structure (especially for B–B contacts) but flatten to unity by 5 Å, indicating a homogeneous melt without long-range segregation. The dihedral histogram spans the full 360 ° range, confirming that low torsional barriers preserve backbone flexibility even in the restricted volume.

Overall, the cube provides an efficient compromise: it accelerates equilibration, reduces noise, and leaves mean structural and energetic properties unchanged. These findings suggest that modest confinement is a practical strategy for future parameter scans or longer simulations, where quicker convergence and tighter statistical bounds translate directly into lower computational cost.